Optical Absorption Due to Space-Charge-Induced Localized States

C. B. DUKE
General Electric Research and Development Center, Schenectady, New York
(Received 3 March 1967)

A self-consistent model of the space-charge potential in narrow, degenerate accumulation regions at a planar semiconductor interface is constructed and applied to evaluate the binding energies and wave functions of quantized, localized states for motion normal to the interface. The model attributes the space-charge potential entirely to charge trapped in the two-dimensional energy bands associated with the localized states. Expressions are derived for the contributions to the absorption coefficient due to vertical transitions among the two-dimensional bands and due to interband transitions in which either the initial or final state is localized near the interface. The results of numerical calculations are presented for n-type accumulation regions in GaAs and at the (100) surface of silicon. Experimental observation of the structure in the absorption coefficient at infrared frequencies appears to be practical, and would provide a direct observation of quantization effects in narrow accumulation or inversion channels at semiconductor surfaces.

I. INTRODUCTION

ALTHOUGH the customary analyses[1] of accumulation and inversion layers at semiconductors interfaces are based on the semiclassical Fermi-Thomas model of the charge distributions in these layers, the possible importance of the quantum nature of the one-electron eigenstates in such regions has been recognized for at least ten years.[2] Most of the experimental data interpreted as giving evidence for such quantized states are measurements of carrier mobilities at semiconductor surfaces.[3–6] However, serious extensions of the bulk-mobility calculations to surfaces[7] have considered primarily the modifications of the mobility by scattering from the surface. The effects of the quantization of the single-particle motion normal to the interface has been investigated only for a quasiclassical limit[7] in which it acts to widen the space-charge region. Although an application of the Kubo formalism to examine alterations in the influence of the exclusion principle on transport properties in a two-dimensional system is in progress,[8] a quantitative interpretation of the experimental conductivity and mobility data has not been given.

More recently, it has been suggested[9] that tunneling into and out of these quantized ("localized") states in narrow accumulation regions contributes characteristic structure to the differential conductance of semimetal (semiconductor)–oxide–metal tunnel junctions. Although experimental data[10] on semimetal junctions can be qualitatively interpreted in terms of this model, the interpretation is not unequivocal owing both to uncertainties in the band structure and space-charge region of the semimetal[9] and to indications that the data themselves may not be typical of such tunnel junctions.[11]

In this paper we propose that experiments[12] on the absorption of electromagnetic radiation from far-infrared to optical frequencies provide a more direct and sensitive probe of the localized states than do measurements of transport properties. Furthermore, absorption measurements are more easily interpreted than those of tunnel conductance. The quantization of motion normal to the interface contributes characteristic structure to the absorption coefficient in the infrared due to transitions among the two-dimensional localized-state energy bands and in the visible due to modifications of the Franz-Keldysh effect[13] near the junction by the presence of these two-dimensional energy bands at energies below the bulk band gap. The two types of transitions are indicated schematically in Fig. 1 by the nomenclature "1" and "2", respectively. The figure, drawn to illustrate an n-type accumulation region in a direct band-gap semiconductor like GaAs, also shows the shape of the space-charge region and the the density of states $\rho_{11}(E+E_i)$ associated with quan-

[1] See, e.g., A. Many, Y. Goldstein, and N. B. Grover, *Semiconductor Surfaces* (North-Holland Publishing Company, Amsterdam, 1965), Chap. 4.

[2] J. R. Schrieffer, *Semiconductor Surface Physics*, edited by R. H. Kingston (University of Pennsylvania Press, Philadelphia, Pennsylvania, 1957), p. 68; J. F. Deward, Ann. N. Y. Acad. Sci. **101**, 872 (1963).

[3] P. Handler and S. Eisenhouer, Surface Sci. **2**, 64 (1964); F. Proix and P. Handler, *ibid.* **5**, 81 (1966).

[4] N. St. J. Murphy, Surface Sci. **2**, 86 (1964).

[5] F. F. Fang and W. E. Howard, Phys. Rev. Letters **16**, 797 (1966).

[6] A. B. Fowler, F. F. Fang, W. E. Howard, and P. J. Stiles, Phys. Rev. Letters **16**, 901 (1966); J. Phys. Soc. Japan, Suppl. **21**, 331 (1966).

[7] A synopsis of these calculations has been given by R. F. Greene, Surface Sci. **2**, 101 (1964).

[8] C. B. Duke (to be published) and F. Stern and W. E. Howard (to be published) have used a Boltzmann-equation approach to calculate the impurity-scattering mobility in the limit that only one localized-state band contains carriers. Their results differ from those of the Kubo treatment in this limit due to phase factors which occur when an average over a random distribution of impurities normal to the surface is taken.

[9] D. J. BenDaniel and C. B. Duke, General Electric Research and Development Center Report No. 66-C-331 (1966) (to be published).

[10] L. Esaki and P. J. Stiles, Phys. Rev. Letters **14**, 202 (1965); **16**, 574 (1966).

[11] I. Giaever (private communication).

[12] Such experiments are currently being undertaken by W. Engeler and M. Garfinkel.

[13] See, e.g., K. Tharmalingham, Phys. Rev. **130**, 2204 (1963).

tized motion normal to the interface. The unhindered motion in the two directions parallel to the plane of the junction is responsible for creating a two-dimensional energy band from the localized-state normal to the junction.[14] As in our analysis of tunneling,[9] we construct models in which the motion normal and parallel to the junction is separable. The density of states in such models is of the form illustrated in Fig. 1 with additional structure at higher energies in both the continuum (ρ_c) and two-dimensional (ρ_{11}) density of states. A schematic illustration of the high-energy structure in the two-dimensional density of states and its relation to the three-dimensional continuum density of states if shown schematically in Fig. 2 for an s band in a simple tetragonal lattice. The structure is associated with symmetry points as indicated in the figure,[15] if the junction is taken parallel to the yz plane, and the axis of fourfold symmetry is taken along the z axis. In the tight-binding approximation, motion parallel and normal to the plane of the junction are identically separable so that the entire structure in ρ_{yz} would be mirrored in tunneling and optical-absorption measurements. To the extent that such consideration apply to more complicated band structures, these measurements can provide an additional source of information about the bulk band structure as well as surface properties of various materials.

The performance of optical-absorption experiments to measure the properties of the surface region of a semiconductor is a familiar idea. Harrick[16] has developed experimental techniques for studying and analyzing absorption at the surface due to both free carriers and surface states. Optical absorption in layered materials, like GeS, GaSe, and MoS_2, is often interpreted as reflecting the band structure of a two-dimensional system[17–19] similar to that associated with the localized-state bands. In particular, phase-sensitive-detection techniques developed to measure, analyze and separate the contributions to the absorption from free carriers and conventional surface states are applicable also to the investigation of quantization effects in narrow space-charge channels. The binding energies and oscillator strengths associated with these states are sensitive functions of the parameters of both the space-charge potential and the bulk semiconductor sample. Our objective in this paper is the development of a tractable model of the space-charge region near a field-plate, metal-insulator-semiconductor junction and its quantitative application to obtain the energies of the localized states and their contributions to the

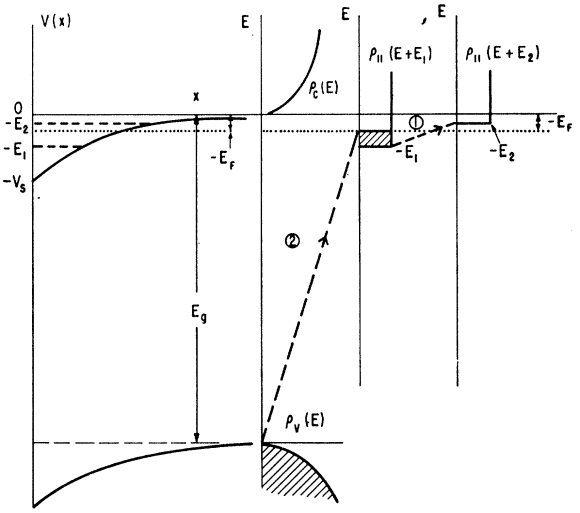

FIG. 1. A schematic illustration of the space-charge region, localized-state energies, E_i, and one-electron density of states associated with a narrow, n-type accumulation region at a semiconductor interface. Infrared transitions between the two-dimensional energy bands associated with the localized states are indicated by the dashed line labeled "1." Interband transitions to one of the localized-state bands are indicated by the dashed line labeled "2."

absorption coefficient. We consider only vertical transitions among the localized-state two-dimensional bands and the effects of these bands on the conventional interband absorption. Exciton correlations[19] are neglected. In Sec. II we derive the quantization condition for the localized states, develop a self-consistent model for the space-charge potential, and apply this model to the numerical calculation of the localized-state energies for degenerate n-type accumulation regions in GaAs and Si. Section II ends with a derivation of the continuum valence-band wave functions for which the space-charge potential induces a depletion region. These wave functions are utilized in Sec. III to calculate the effect of

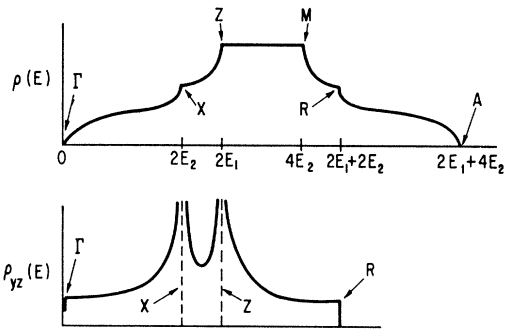

FIG. 2. A schematic illustration of the continuum density of states $\rho(E)$ associated with an s band in a simple tegragonal lattice. The letters refer to the symmetry points as given, e.g., in Ref. 15. The density of states $\rho_{yz}(E)$ is that associated with a plane passing through the fourfold (z) axis of the tetragonal Brillouin zone and parallel to one of the rectangular faces of the Brillouin zone. The E_β labels correspond to the parameters in the tight-binding approximation energy band $\epsilon(\mathbf{k})=E_1[1-\cos(k_x a_1)]+E_2[2-\cos(k_x a_2)-\cos(k_y a_2)]$.

[14] This situation is familiar from the conventional theory of Tamm and Shockley states. See, also, V. Heine, Phys. Rev. **138**, A1689 (1965); Surface Sci. **2**, 1 (1964).

[15] G. F. Koster, Solid State Phys. **5**, 173 (1957).

[16] N. J. Harrick, Phys. Rev. **125**, 1165 (1962); see also Ref. **1**, pp. 292–295.

[17] J. L. Brebner, J. Phys. Chem. Solids **25**, 1927 (1965).

[18] R. F. Frindt, Phys. Rev. **140**, A536 (1965).

[19] H. I. Ralph, Solid State Commun. **3**, 303 (1965).

localized states on interband absorption. We conclude with the derivation of the steplike structures in the absorption coefficient at infrared frequencies due to vertical transitions among the two-dimensional energy bands associated with the localized states, and a synopsis of our results.

II. EIGENFUNCTIONS AND EIGENVALUES IN THE SPACE-CHARGE REGION

A. Localized States in Accumulation (Inversion) Layers

We consider a planar metal-insulator-semiconductor junction of either the tunneling (thin-oxide) or field-plate (thick-oxide) type. The effective-mass approximation[20] is used to evaluate the one-electron wave functions inside the semiconductor. Therefore they are given by

$$\psi_E(\mathbf{r})=\sum_{\mathbf{k}} f_{j,E}(\mathbf{k})\psi_{\mathbf{k},j}(\mathbf{r}), \tag{2.1a}$$

$$f_{j,E}(\mathbf{k})=N^{-1/2}\int d^3r e^{i\mathbf{k}\cdot\mathbf{r}} f_{j,E}(\mathbf{r}), \tag{2.1b}$$

in which $\psi_{\mathbf{k},j}(\mathbf{r})$ denotes the Bloch functions of the bulk semiconductor, and N is the number of unit cells in the crystal. In a previous paper[21] we demonstrated that if the effective-mass approximation is valid in both the semiconductor and oxide, then the wave functions near the junction are obtained by solving the effective-mass Schrödinger equation for the envelope functions $f_{j,E}(\mathbf{r})$ with the boundary conditions of continuity of f and of $m^{-1}(df/dx)$ at the junction interfaces. The potential used in Refs. 9 and 21 to calculate the wave functions consists of a uniform potential in the metal and oxide together with an exponential potential in the semiconductor. More generally, the potential in the oxide consists of a uniform electric force field F (in eV/cm), superposed on a uniform potential attributed to the difference between the oxide and semiconductor electron affinities. Thus we write

$$\begin{aligned} V(x)&=-V_m, && x<-x_j \\ &=V_b+Fx, && -x_j<x<0 \\ &=-V_s\exp(-gx), && 0<x, \end{aligned} \tag{2.2}$$

where x_j is the oxide thickness, g is the decay constant of the space-charge region in the semiconductor, and $V_b=\chi_s-\chi_{ox}$ is the barrier height at the semiconductor-oxide interface in the absence of band bending ($V_s=0$). The quantities F, V_s, and g are related via Gauss's law at the semiconductor-oxide interface as discussed in part B to follow and Appendix B of Ref. 21.

The effective-mass equation for the envelope function $f_{c,E}(\mathbf{r})$ in the (accumulated: $V_s>0$) conduction band can be written as

$$f_{c,E}(\mathbf{r})=\frac{\exp(i\mathbf{k}_{\|,c}\cdot\boldsymbol{\varrho})}{A^{1/2}}\phi_{\mathcal{E}_c}(x), \tag{2.3a}$$

$$E_c=\frac{\hbar^2}{2}\left[\frac{k_{\|,c,2}^2}{m_{\|,2}}+\frac{k_{\|,c,3}^2}{m_{\|,3}}\right]+\mathcal{E}_c, \tag{2.3b}$$

$$\left[\frac{d^2}{dx^2}+Q_c^2e^{-gx}+\frac{2m_{\perp,c}\mathcal{E}_c}{\hbar^2}\right]\phi_{\mathcal{E}_c}(x)=0, \tag{2.3c}$$

$$Q_c^2=2m_{\perp,c}V_s/\hbar^2. \tag{2.3d}$$

The junction is taken normal to a symmetry axis of the crystal such that all the effective-mass ellipsoids have principal axes ($m_{\perp,c}$) normal to the junction. The quantities $m_{\|,c,1}$ and $m_{\|,c,2}$ are the masses associated with motion parallel to the plane of the junction; and A is the area of the junction. The solutions to (2.3c) are given by[21]

$\mathcal{E}_c>0$:

$$\phi(x)=\alpha_+\phi_+(x)+\alpha_-\phi_-(x), \tag{2.4a}$$

$$\phi_\pm(x)=F(-Q_c^2, g, \pm ip_c, x), \tag{2.4b}$$

$$p_c=2k_c/g, \tag{2.4c}$$

$$k_c^2=2m_{\perp,c}\mathcal{E}_c/\hbar^2. \tag{2.4d}$$

$\mathcal{E}_c<0$:

$$\phi_+(x)=\alpha_+F(-Q_c^2, g, -p_c, x), \tag{2.5a}$$

$$p_c=2q_c/g, \tag{2.5b}$$

$$q_c^2=-2m_{\perp,c}\mathcal{E}_c/\hbar^2, \tag{2.5c}$$

$$\begin{aligned} F(-Q^2, g, p, x) &\equiv\exp(pgx/2)\sum_{n=0}^{\infty}\left(\frac{-Q^2e^{-gx}}{g^2}\right)^n\frac{\Gamma(-p+1)}{n!\Gamma(n-p+1)} \\ &=\Gamma(-p+1)J_{-p}(2Qe^{-gx/2}/g)(Q/g)^p. \end{aligned} \tag{2.6}$$

In Eq. (2.6) $J_p(x)$ is the Bessel function[22] and $\Gamma(p)$ is the (complex) gamma function.[23] The function F and its derivatives are generated numerically[21] from the power-series expansion (2.6). The phases in $\phi_\pm(x)$ are taken to make these functions the one-dimensional Jost functions in which $k_c\to iq_c$ gives the transition from positive to negative energies for normalizable functions.

Our main concern is optical absorption in the semiconductor near the interface. Therefore, we neglect the loss of electrons via tunneling through the oxide and impose the boundary condition that the envelope function in the oxide is purely decaying in character. The Schrödinger equation for the envelope function in the oxide (for a spherical mass ellipsoid with associated mass, m_b) is given by

$$\frac{d^2\phi}{dx^2}-\frac{2m_b}{\hbar^2}(V_b+Fx-\mathcal{E}_c)\phi=0. \tag{2.7}$$

[20] W. Kohn, Solid State Phys. **5**, 258 (1957).
[21] D. J. BenDaniel and C. B. Duke, Phys. Rev. **152**, 683 (1966).
[22] F. W. J. Oliver, Natl. Bur. Std. Appl. Math. Ser. **55**, 355 (1964).
[23] P. J. Davis, Natl. Bur. Std. Appl. Math. Ser. **55**, 253 (1964).

Equation (2.7) has the general solution[24]

$$\phi(x)=\beta_+ \mathrm{Ai}(\xi)+\beta_- \mathrm{Bi}(\xi), \tag{2.8a}$$

$$\xi=k_F[x-(\mathcal{E}_c-V_b)/F], \tag{2.8b}$$

$$k_F\equiv(2m_bF/\hbar^2)^{1/3}=1.382\times10^5F^{1/3}\ \mathrm{cm}^{-1}. \tag{2.8c}$$

The $\mathrm{Ai}(\xi)$ and $\mathrm{Bi}(\xi)$ are linearly-independent solutions to Airy's equation.[24] The requirement that the envelope function be purely decaying in the oxide is that $\beta_+=0$. The normalizability of the wave function in the semiconductor has been guaranteed by the use of only $\phi_+(x)$ in (2.5a). The equality of the logarithmic derivatives at the boundary gives the bound-state quantization condition for $\mathcal{E}_c<0$.

$$\frac{F'(-Q_c^2, g, -p_{ci}, 0)}{F(-Q_c^2, g, -p_{ci}, 0)}=\left(\frac{m_ck_F}{m_b}\right)\frac{\mathrm{Bi}'(\xi_0)}{\mathrm{Bi}(\xi_0)}, \tag{2.9a}$$

$$\xi_0\equiv\left(\frac{V_b+|\mathcal{E}_c|}{F}\right)k_F. \tag{2.9b}$$

As for sensible parameters even a field-plate device exhibits $\xi_0\gg1$; we use the asymptotic expansions for the Airy functions[24] to obtain

$$\left(\frac{m_ck_F}{m_b}\right)\frac{\mathrm{Bi}'(\xi_0)}{\mathrm{Bi}(\xi_0)}\overset{\xi_0\gg1}{\rightarrow}\frac{m_ck_F\xi_0^{1/2}}{m_b}$$

$$=\frac{m_c}{m_b}\left[\frac{2m_b}{\hbar^2}(V_b+|\mathcal{E}_c|)\right]^{1/2} \tag{2.9c}$$

which makes (2.9a) identical to the form found in Ref. 9 for a square-barrier model of the oxide. We emphasize that if $\xi_0\gg1$, Eq. (2.9c) indicates that the bound-state eigenvalues in the accumulated conduction band are independent of the electric field in the oxide when V_s assumes a fixed value. Therefore the entire influence of the field-plate bias on the eigenvalue condition (2.9) occurs because the bias determines the shape of the space-charge region (i.e., both V_s and g) via an appropriate Poisson equation.

The final preliminaries consist of determining α_+ in (2.5a) from the normalization of the envelope functions

$$\int_{-\infty}^{\infty}\phi_{\mathcal{E}}(x)\bar{\phi}_{\mathcal{E}'}(x)dx=\delta_{\mathcal{E},\mathcal{E}'},\quad \mathcal{E}<0 \tag{2.10}$$

and discussing tractable approximations to integrals needed in considerations of oscillator strengths of various transitions. We first note that when $\xi_0\gg1$ in (2.9), we can neglect the contribution to integrals from $x<0$ (in the oxide) to an accuracy of usually better than 1%. In fact one can derive closed-form expressions from the integral in (2.10) in terms of Bessel and gamma functions if we take the $V_b\rightarrow\infty$ limit so that (2.9a) becomes

$$F(-Q_c^2, g, -p_{ci}, 0)=0,\quad V_b\rightarrow\infty. \tag{2.9d}$$

However, these expressions are not useful for computations because they involve differentiation of Bessel and gamma functions with respect to order and argument, respectively. Therefore we use the power-series expansion given in Eq. (A6) of the Appendix to write from (2.5a) and (2.10)

$$\alpha_+^{-2}(p_c)=-\frac{2}{g}\sum_{m=0}^{\infty}\frac{1}{m!}\left(\frac{-Q_c^2}{g^2}\right)^m\frac{\Gamma(2p_c+2m)}{\Gamma(2p_c+m+1)}$$

$$\times\left[\frac{\Gamma(p_c+1)}{\Gamma(p_c+1+m)}\right]^2. \tag{2.11}$$

The leading term in the expansion gives

$$\alpha_+^{-2}\cong1/gp_c=1/2q_c, \tag{2.12}$$

which is the result obtained by approximating $\phi_+(x)$ by a simple exponential with the decay constant associated with the binding energy of the eigenstate. Equation (2.12) gives an excellent approximation to α_+ for any bound state in "shallow" potentials $(Q_c/g)\ll1$ or loosely bound states, $p_c\ll1$, in any potential. We also evaluate the matrix element relevant for dipole-allowed absorption between two localized-state bands.

$$\langle f|p_x|i\rangle=\frac{\hbar}{i}\int_0^{\infty}\phi_{\mathcal{E}_f}(x)\frac{d}{dx}\phi_{\mathcal{E}_i}(x)dx,$$

$$=\frac{\hbar}{i}\alpha_+(p_{cf})\alpha_+(p_{ci})I_3(-p_{cf}, -p_{ci}), \tag{2.13}$$

with $I_3(-p_{cf}, -p_{ci})$ given by Eq. (A14) in the Appendix. Taking the leading term of the expansions for both α_+ and I_3 we get

$$\langle f|p_x|i\rangle\cong\frac{4\hbar}{i}(q_{cf}q_{ci})^{1/2}\frac{q_{ci}}{q_{ci}+q_{cf}}, \tag{2.14a}$$

$$\langle i|p_x|f\rangle\langle f|p_x^{\dagger}|i\rangle\cong16\hbar^2\left[\frac{(q_{cf}q_{ci})}{(q_{cf}+q_{ci})}\right]^2. \tag{2.14b}$$

Equation (2.14b) is used in Sec. III to approximate the oscillator strength for transitions between localized bands associated with the states at energies $\mathcal{E}_i=-\hbar^2\times(2p_{ci}g)^2/2m_{\perp,c}$ and $\mathcal{E}_f=-\hbar^2(2p_{cf}g)^2/2m_{\perp,c}$. It is a valid approximation when Eq. (2.12) gives an accurate normalization integral for both states.

B. Self-Consistant Capacitor Model for a Field-Plate Geometry

A complete model of the semiconductor-oxide-metal electrostatic potential requires specification of the detailed surface-charge density in the oxide near the

[24] H. A. Antosiewicz, Natl. Bur. Std. Appl. Math. Ser. **55**, 435 (1964).

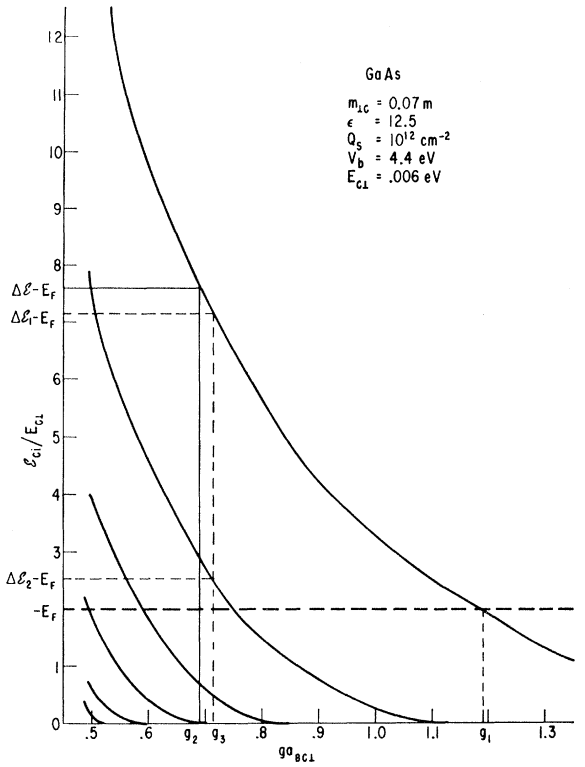

FIG. 3. Localized-state binding energies for accumulation regions satisfying Eq. (2.15) with $Q_s=10^{12}$ cm^{-2} in GaAs. The horizontal heavy dashed line indicates a hypothetical Fermi energy of -12 meV. The lightly dashed and light solid lines indicate constructions used in determining the self-consistent potential as discussed below Eqs. (2.16) in the text. The localized-state eigenvalues are obtained by solving Eq. (2.9a) in the text using the parameters indicated in the figure.

semiconductor surface. In terms of such a model, the parameters of the space-charge potential, V_s and g in Eq. (2.2), can be determined as a function of the voltage applied across the junction by solving Poisson's equation.[1,21] For an accumulated surface, the relevant parameter characteristic of the bulk semiconductor is the total mobile charge per unit area, Q_s. Therefore we use Q_s rather than the applied bias to characterize the space-charge region. From Gauss's law, the derivative of the electrostatic potential is related to the charge Q_s via

$$\left(\frac{dV}{dx}\right)_{x=0} = V_s g = \frac{4\pi Q_s}{\epsilon}, \tag{2.15}$$

in which ϵ is the dielectric constant of the semiconductor. Thus each value of Q_s specifies a family of possible space-charge potentials whose range and depth are related by (2.15). The self-consistent potential is that member of the family which traps just the (measured) total charge per unit area Q_s. Therefore the final self-consistent potential depends on the properties of the particular bulk sample under consideration as well as on the band bending in the surface region.

In order to get widely spaced ($\Delta E \gtrsim 10$ meV) localized states suitable for direct observations by optical absorption, we consider values of Q_s which lead to relatively deep, narrow accumulation regions. The total mobile charge density consists of contributions from the carriers in the bulk material and from the charge trapped in the accumulation regions. A fully self-consistent model of the space-charge-induced band bending in the semiconductor requires the consideration of both contributions to the charge density and hence a detailed specification of the carrier statistics in the bulk sample. In order to avoid lengthy considerations of a variety of bulk-semiconductor statistics (which considerations are largely irrelevant for our present purposes anyway), we devise approximation procedures to estimate the space-charge potential. The fundamental approximation, common to both of the procedures we utilize, is that for narrow, degenerate accumulation regions, the total mobile charge Q_s can be replaced by only the contribution to it due to charge trapped in the accumulation region. If the bulk-carrier contributions to the charge density were truly negligible, then for a fixed value of V_s, g could be determined by calculation of the asymptotic form of $V(x)$ as $x \to \infty$ from Poisson's equation using as a source the charge density obtained from asymptotic form of the wave functions of the trapped charge. The quasi-Fermi energy E_F in the accumulation region is determined by condition that the total trapped charge density be Q_s. The inadequacy of this approximation in a particular sample is reflected in the fact that the E_F calculated by the above procedure does not in general equal the bulk Fermi energy. If we considered an initial-value problem using the above-calculated trapped charge and space-charge potential, we would find that as time progresses, charge leaks out of the space-charge region until E_F equals the bulk Fermi energy, and that usually the space-charge potential simultaneously becomes wider. This observation motivates our second estimation procedure for the range of the potential in which E_F is taken as fixed at the bulk value, and the parameter g is determined by the requirement that the trapped charge be equal to Q_s. These "self-consistent" estimation schemes are discussed subsequently in more detail. They exhibit the attractive feature that for their application the only property of the bulk sample that is needed is its bulk Fermi energy.

The charge density in narrow accumulation regions is usually well approximated as a series of two-dimensional degenerate Fermi gases for temperatures (T) near 77° and below. Unfortunately, the extensive literature[1] on the shape of the space-charge region and charge distribution at semiconductor interfaces is of no direct assistance in our analysis. In this literature the space-charge region is treated as a three-dimensional Fermi gas in which the quantization effects which we are studying have been neglected. Using degenerate Fermi

statistics at $T=0$, the total charge trapped by the two-dimensional energy bands with $E_c<E_F$ is given by

$$Q_s=\sum_{i,\beta}\rho_{\parallel}^{(\beta)}(E_F+\mathcal{E}_{ci}^{(\beta)})\Theta(E_F+\mathcal{E}_{ci}^{(\beta)}), \quad (2.16a)$$

$$\Theta(x)=1, \quad x>0$$
$$=0, \quad x<0, \quad (2.16b)$$

$$\mathcal{E}_{ci}^{(\beta)}=+\hbar^2(gp_{ci}^{(\beta)})^2/8m_{\perp,c}^{(\beta)}, \quad (2.16c)$$

$$\rho_{\parallel}^{(\beta)}=(2j^{(\beta)}+1)n^{(\beta)}(m_{\parallel,c,1}m_{\parallel,c,2})^{1/2}/2\pi\hbar^2, \quad (2.16d)$$

in which $n^{(\beta)}$ is taken to be the number of equivalent ellipsoids of the βth type containing charge in localized states. The quantum number β denotes the various sets of inequivalent ellipsoids relative to a particular surface in a many-valley semiconductor. The $p_{ci}^{(\beta)}$ are the eigenvalues obtained from Eqs. (2.9) for the β set of ellipsoids. The effective spin of the ellipsoids is taken to be $j^{(\beta)}$ which, evidently, is not always $\frac{1}{2}$ for degenerate valence bands associated with p-type accumulation regions. It should be emphasized that Eqs. (2.16), and our entire analysis, are valid only if the motion parallel to the semiconductor surface is separable from the motion normal to the surface. In particular this separation does not occur for n-type accumulation regions on the (111) surfaces of Si. This fact may account for the failure to observe evidence of quantized states associated with these surfaces.[5,6]

We conclude this part of Sec. II by outlining the two procedures to estimate the parameters of the self-consistent space-charge potential and presenting calculations of the binding energies of the bound states in various families of potentials which satisfy Eq. (2.15). We illustrate the procedures in a case in which only a few localized states contain electrons. In Figs. 3 and 4 we show the possible binding energies, $\mathcal{E}_{ci}=-\mathcal{E}_i$, of the localized states associated with the conduction band of GaAs for $Q_s=10^{12}$ cm^{-2} and 10^{13} cm^{-2}, respectively. Energies are measured in units of the (normal-motion) shallow-donor binding energy, $E_{c1}\equiv\hbar^2/2m_{\perp,c}a_{Bc1}^2$, and distances in units of the conduction-band Bohr radius for motion normal to the interface; $a_{Bc1}\equiv\hbar^2\epsilon/m_{\perp,c}e^2$. Let us consider in detail the case of $Q_s=10^{12}$ cm^{-2} for a bulk Fermi energy of $E_F=-2E_c=-0.012$ eV. A vertical line drawn at a particular value of ga_{Bc1} in Fig. 3 intersects the solid curves at the binding energies $\mathcal{E}_{ci}/E_{c1}$ of the localized states in a space-charge potential of range g^{-1} and depth obtained from Eq. (2.15). These energies are calculated by graphical solution of Eq. (2.9a) using the parameters indicated in the figures. As g decreases from right to left in the figures, the potential becomes both wider and deeper because of Eq. (2.15). Therefore both the binding energies and the number of bound states increase as the value of g diminishes.

As discussed below Eq. (2.15), we can construct an estimate of the range of the potential by assuming its

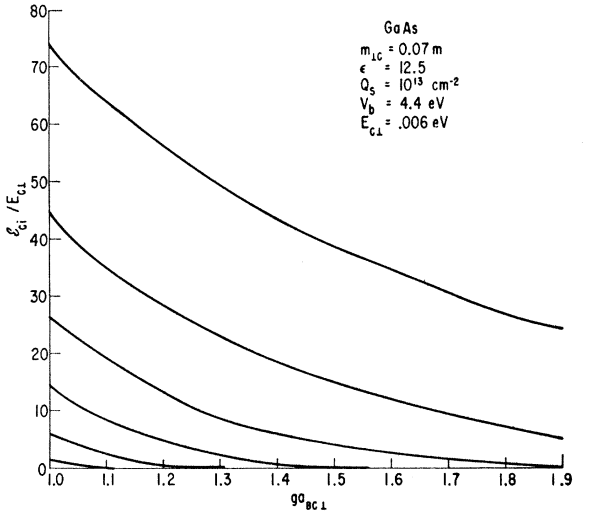

FIG. 4. Localized-state binding energies for n-type accumulation regions in GaAs satisfying Eq. (2.15) with $Q_s=10^{13}$ cm^{-2}. The eigenvalues are obtained by solving Eq. (2.9a) using the parameters indicated in the figure.

asymptotic form to be determined by the spatial distribution of the trapped charge. This estimate is given by

$$g_0a_{Bc1}=2\mathcal{E}_0^{1/2}, \quad (2.17a)$$

in which $\mathcal{E}_0$ denotes the energy of the least tightly bound occupied localized state. The total accumulated charge Q_s in the potential determines the quasi-Fermi level E_F via

$$\Delta\mathcal{E}=\sum_i(\mathcal{E}_{ci}+E_F)/E_{c1}=Q_s/\rho_{\parallel}E_{c1}$$
$$=Q_s/(1.78\times10^{11}) \quad : \quad \text{GaAs}. \quad (2.17b)$$

For $Q_s=10^{12}$ cm^{-2}, Eq. (2.17b) requires $\Delta\mathcal{E}=5.62$ in GaAs. The satisfaction of (2.17a) is determined graphically from Fig. 3. Several solutions may exist which correspond to varying numbers of bound states being occupied. If only the lowest-energy bound state is occupied we find $g_0a_{Bc1}\sim1.6$, and $E_F\cong5E_{c1}$. However, if the second bound state also is occupied, we obtain $g_0a_{Bc1}\cong1.0$ and $E_F\cong0.75E_{c1}$. More than two bound states cannot be occupied if (2.17a) is satisfied simultaneously with (2.17b) for $Q_s=10^{12}$ cm^{-2}. The smallest estimate for the range of the potential is that obtained when only the lowest-energy state is occupied.

An estimate of the upper bound on the range of the potential is obtained by recalling that the total mobile charge is due to both bulk and trapped charge. In the limit that equilibrium between the accumulation layer and bulk material has achieved, the charge trapped in the accumulation region is determined by the bulk Fermi level which also is denoted by E_F. If we use E_F as given in Eq. (2.17b) and neglect the difference between the total mobile charge and that trapped in the accumulation region, then (2.17b) determines the

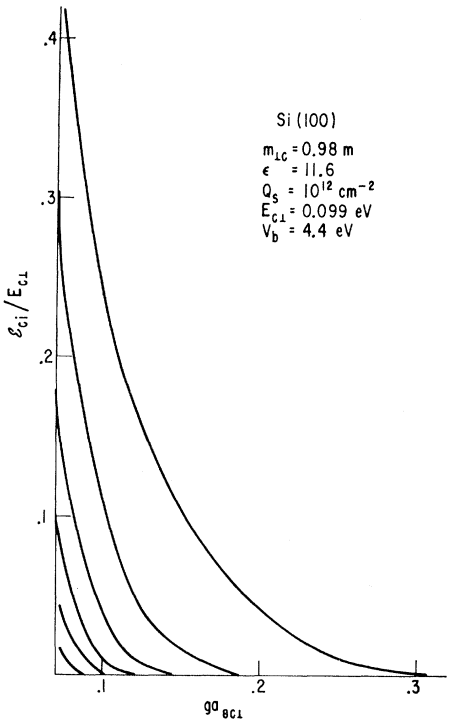

FIG. 5. Localized-state binding energies associated with the ⟨100⟩ ellipsoids in Si for n-type accumulation regions on the (100) face satisfying Eq. (2.15) with $Q_s=10^{12}$ cm^{-2}. The eigenvalues are obtained by solving Eq. (2.9a) using the parameters indicated in the figure.

range g of the potential that just traps the charge Q_s. This procedure usually overestimates the effective range of the potential near the interface because it requires the estimated potential to trap more charge than does the actual space-charge potential. As wide accumulation regions exhibit more closely spaced localized-state energies, this latter estimation scheme is more restrictive, hence more useful, than the former one. Making the application to GaAs, we see that the "self-consistent" g must be smaller than g_1, illustrated in Fig. 3, which is the decay constant at which the lowest localized-state energy is at the (bulk) Fermi energy. We recall that for $Q_s=10^{12}$ cm^{-2}, Eq. (2.17b) requires that $\Delta\mathcal{E}=5.62$ for a single localized state. This requirement gives the inverse range g_2 indicated in Fig. 3. However, for $ga_{Bc\perp}<0.75$ two localized states lie below the Fermi energy so we require that the sum of their heights, $\Delta\mathcal{E}_1$, and $\Delta\mathcal{E}_2$, respectively, gives the total required number of occupied states, i.e., from Eq. (2.17) $\Delta\mathcal{E}=\Delta\mathcal{E}_1+\Delta\mathcal{E}_2$. This construction shown in Fig. 3 with lightly dashed lines, gives the inverse range $g_3a_{Bc\perp}=0.715$ and depth obtained from (2.15). The space-charge region contains three localized states with 41-, 15-, and 3-meV binding energies. The 41 and 15 meV bands are filled up to the Fermi energy of -12 meV, and the 3-meV band is completely empty. Noting that $\Delta\mathcal{E}$ scales linearly with Q_s, via Eq. (2.17), we employ a correspondingly larger energy scale in Fig. 4 for $Q_s=10^{13}$ ($\Delta\mathcal{E}=56.2$) than in Fig. 3 for $Q_s=10^{12}$ ($\Delta\mathcal{E}=5.62$).

As measurements of transport properties at accumulated (100) surfaces of silicon indicate the presence of localized-state bands,[5,6] these surfaces are of particular interest as an example of the above analysis. The two electron ellipsoids whose long axes lie in the ⟨100⟩ directions are inequivalent to the other four. For these two ellipsoids, $m_{\perp c}=0.98m$ and $m_{\parallel,c,1}=m_{\parallel,c,2}=0.19m$, whereas for the other four ellipsoids $m_{\perp c}=0.19m$, $m_{\parallel,c,1}=0.19m$, and $m_{\parallel,c,2}=0.98m$. Therefore the localized states associated with the two ⟨100⟩ ellipsoids have less kinetic energy and therefore greater binding energy in the same space-charge potential.[5] Figures 5 and 6 illustrate the binding energy versus space-charge-potential curves for the ⟨100⟩ ellipsoids using $Q_s=10^{12}$ and 10^{13} cm^{-2}, respectively. The equation which relates the self-consistent potential to the trapped charge, analogous to (2.17b) for GaAs but accounting for the occurrence of two equivalent ellipsoids, is

$$\Delta\mathcal{E}=Q_s/(1.574\times10^{13}),\quad \text{Si } \langle100\rangle \text{ ellipsoids.} \quad (2.18)$$

Therefore $\Delta\mathcal{E}=0.0635$ for $Q_s=10^{12}$ cm^{-2} and $\Delta\mathcal{E}=0.635$ for $Q_s=10^{13}$ cm^{-2}. Inspection of Figs. 5 and 6 indicates that only the lowest two-dimensional band contains electrons for almost any bulk Fermi energy E_F. This result is consistent with the model used by Fang and Howard.[5] However for $|E_F|/E_{c\perp}\gtrsim1$ (e.g., 200Ω cm

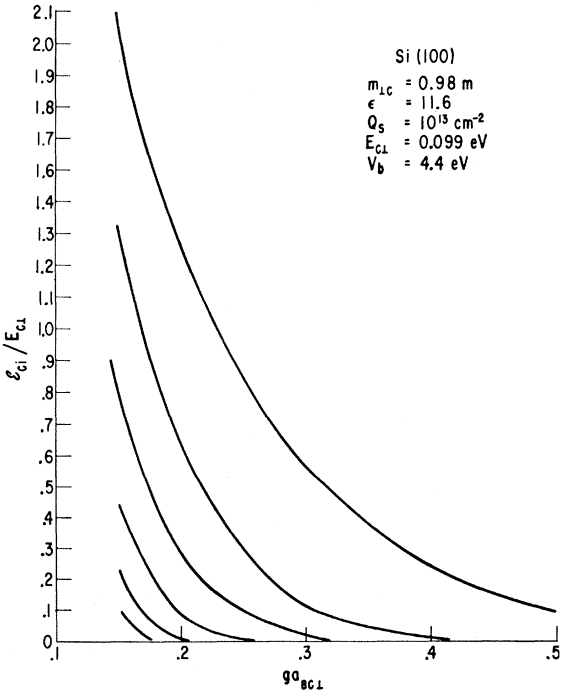

FIG. 6. Localized-state binding energies associated with the ⟨100⟩ ellipsoids in Si for n-type accumulation regions on the (100) face satisfying Eq. (2.15) with $Q_s=10^{13}$ cm^{-2}. The eigenvalues are obtained by solving Eq. (2.9a) using the parameters indicated in the figure.

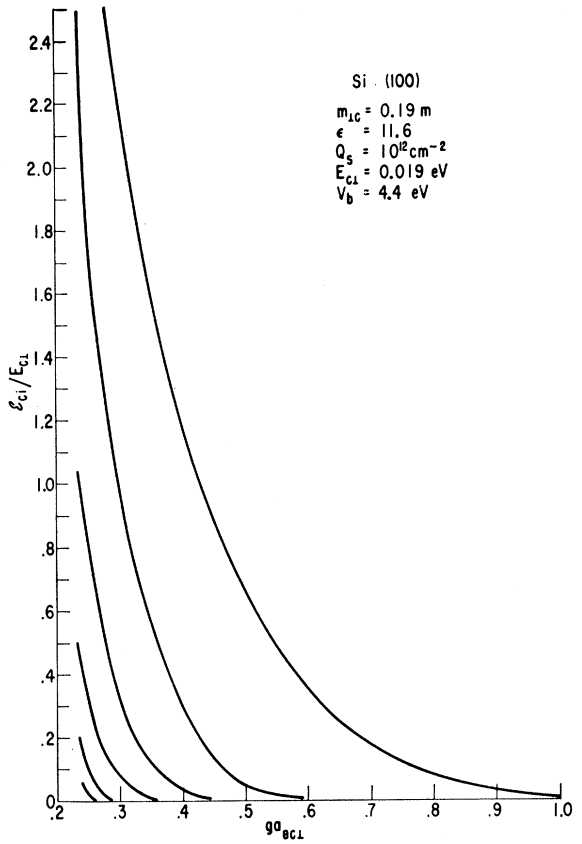

FIG. 7. Localized-state binding energies associated with the ⟨010⟩ and ⟨001⟩ ellipsoids in Si for n-type accumulation regions on the (100) face satisfying Eq. (2.15) with $Q_s=10^{12}$ cm^{-2}. The eigenvalues are obtained by solving Eq. (2.9a) using the parameters indicated in the figure.

Si at 77°K gives $E_F=-80$ meV, $E_F/E_{c1}=-0.8$), we obtain at least five additional unfilled higher-energy bands at $Q_s=10^{13}$ cm^{-2} and approximately 10 for $Q_s=10^{12}$ cm^{-2}.

The binding energy as a function of space-charge potential for the other four (⟨010⟩ and ⟨001⟩) ellipsoids is shown in Figs. 7 and 8 using $Q_s=10^{12}$ and 10^{13} cm^{-2}, respectively. The difference in normal mass values between the two sets of ellipsoids causes the (ga_{Bc1}) axes to differ by a scaling factor

$$(ga_{Bc1})_{\text{eff}}^{(100)}=0.194(ga_{Bc1})^{(010)}, \qquad (2.19)$$

in which $(ga_{Bc1})_{\text{eff}}^{(100)}$ is the "comparable" ⟨100⟩ value of ga_{Bc1} to that obtained from Figs. 7 and 8. The self-consistent-potential criterion, incorporating the effect of all four ellipsoids, is

$$\Delta\mathcal{E}=Q_s/(1.36\times10^{13}): \text{ Si } \langle010\rangle \text{ and } \langle001\rangle \text{ ellipsoids.} \qquad (2.20)$$

We can examine, for a given value of Q_s and E_F, whether or not the ⟨010⟩ and ⟨001⟩ ellipsoids contain charge by computing g without considering them and subsequently inquiring about their occupancy at that value of g. Thus for $Q_s=10^{13}$ cm^{-2} and $E_F=-80$ meV we find from Fig. 6 that $(ga_{Bc1})^{(100)}=0.19$. From Eq. (2.19) we find that $(ga_{Bc1})_{\text{eff}}^{(010)}=0.97$. Inspection of Fig. 8 reveals that for this potential the ⟨010⟩ and ⟨001⟩ ellipsoids contain two localized-state bands of which the lowest has its minimum at the Fermi energy and hence is not yet occupied. Therefore increasing $Q_s>Q_s^c=10^{13}$ cm^{-2} will populate the lowest ⟨101⟩-⟨001⟩ band in our model. This estimate of the crossover value of Q_s^c for $E_F=-80$ meV is to be compared with the quoted value of $Q_s^c=(3-5)\times10^{12}$ cm^{-2} of Fang and Howard, who do not give their bulk Fermi energy. Application of the estimation procedure associated with Eq. (2.17a) gives a value of Q_s^c closer to that of Ref. 5. We see from the above analysis that for $Q_s=10^{12}$ or 10^{13} cm^{-2} the curves in Figs. 5–8 permit the estimation of the space-charge potential and evaluation of localized-state binding energy for any value of the bulk Fermi energy associated with some particular sample. The values of 10^{12} to 10^{13} cm^{-2} of Q_s span the region of experimentally available parameters which give sufficiently widely spaced localized states that detection of these states by optical absorption is practical.

C. Continuum States in Depletion Regions

In order to discuss interband optical absorption near the semiconductor interface, we must calculate the wave

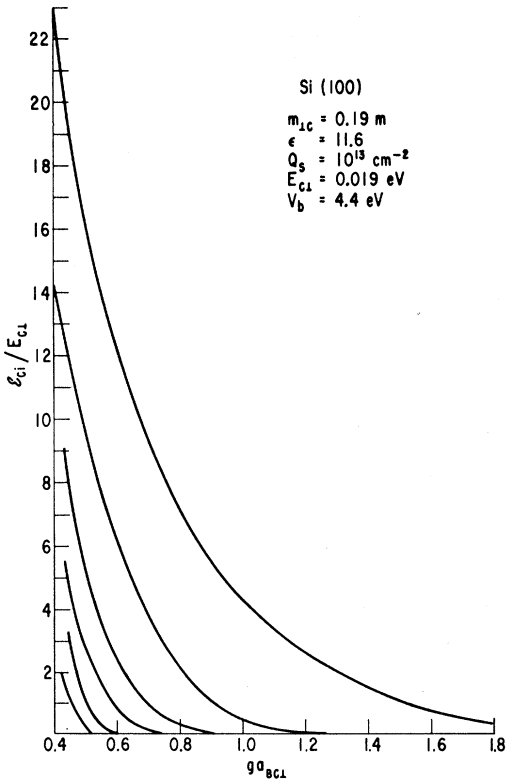

FIG. 8. Localized-state binding energies associated with the ⟨010⟩ and ⟨001⟩ ellipsoids in Si for n-type accumulation regions on the (100) face satisfying Eq. (2.15) with $Q_s=10^{13}$ cm^{-2}. The eigenvalues are obtained by solving Eq. (2.9a) using the parameters indicated in the figure.

functions for bands characterized by a depletion region (in our case the valence band) as well as those characterized by accumulation regions. The calculation is an extension of Tharmalingham's[13] treatment of the Franz-Keldysh effect to the case of an inhomogeneous electric field near the interface.

We consider the eigenstates of a spherical valence (hole) band with mass $-m_v$ in the potential (2.2). The envelope functions of the hole wave functions are given by

$$f_{v,E}(\mathbf{r})=\exp(i\mathbf{k}_{11,v}\cdot\boldsymbol{\varrho})\phi_{\varepsilon_v}(x), \tag{2.21a}$$

$$E_v=-E_g-\frac{\hbar^2 k_{11,v}^2}{2m_v}-\mathcal{E}_v, \tag{2.21b}$$

$$\left[\frac{d^2}{dx^2}-Q_v^2e^{-gx}+\frac{2m_v\mathcal{E}_v}{\hbar^2}\right]\phi_{\varepsilon_v}(x)=0, \tag{2.21c}$$

$$Q_v^2=2m_vV_s/\hbar^2. \tag{2.21d}$$

The top of the valence band lies at energy $-E_g$ relative to the bottom of the conduction band. The general solution to Eq. (2.21c) is

$$\phi_{\varepsilon_v}(x)=d_1F(Q_v^2,g,ip_v,x)+d_2F(Q_v^2,g,-ip_v,x), \tag{2.22a}$$

$$p_v=2k_v/g, \tag{2.22b}$$

$$k_v^2=2m_v\mathcal{E}_v/\hbar^2. \tag{2.22c}$$

The coefficients d_1 and d_2 are determined by the continuity of ϕ and $m^{-1}d\phi/dx$ at the origin using Eqs. (2.8) for the wave functions in the oxide with the boundary condition $\beta_+=0$. In the limit that $V_b\rightarrow\infty$, which is taken for convenience in later evaluating oscillator strengths, we find

$$\phi_{\varepsilon_v}(x)=d_1[F(Q_v^2,g,ip_v,x)-rF(Q_v^2,g,-ip_v,x)], \tag{2.23a}$$

$$r=F(Q_v^2,g,ip_v,0)/F(Q_v^2,g,-ip_v,0). \tag{2.23b}$$

The wave function $\phi_{\varepsilon_v}(x)$ is normalized according to

$$\int_0^\infty \phi_{\varepsilon_v}(x)\bar{\phi}_{\varepsilon_v'}(x)dx=\delta(\mathcal{E}_v-\mathcal{E}_v'), \tag{2.24a}$$

which requires[25]

$$d_1=(m_v/2\pi\hbar^2k_v)^{1/2}. \tag{2.24b}$$

The function $F(Q^2,g,p,x)$ is defined by the series in Eq. (2.6) and is related to the Bessel function of the second kind, $I_p(x)$, by[22]

$$F(Q^2,g,-p,x)=\frac{\Gamma(p+1)}{(Q/g)^p}I_p(2Qe^{-gx/2}/g). \tag{2.25}$$

We later need to know the overlap integral between a localized conduction-band wave function and the continuum valence-band wave function (2.23). Equations (2.5) and (2.23) lead to the result

$$M_{cv}\equiv\int_0^\infty \bar{\phi}_{\varepsilon_c}(x)\phi_{\varepsilon_v}(x)dx=\alpha_+d_1[I_2(-Q_c^2,-p_c;Q_v^2,ip_v)-rI_2(-Q_c^2,-p_c;Q_v^2,-ip_v)], \tag{2.26a}$$

$$I_2(-Q_c^2,-p_c;Q_v^2,ip_v)\equiv\int_0^\infty F(-Q_c^2,g,-p_c,x)\times F(Q_v^2,g,ip_v,x)dx. \tag{2.26b}$$

I_2 is evaluated in the Appendix and is given by Eq. (A8b). A convenient approximation, valid for either p_c, $p_v\lesssim 1$ or $(Q_v/g)\gg 1$, consists of taking only the leading term in Eq. (A8b), and leads to,

$$I_2(-Q_c^2,-p_c;Q_v,ip_v)\cong 2/g(p_c-ip_v)=1/(q_c-ik_v). \tag{2.27a}$$

This approximation also corresponds to setting $r\cong 1$ and $\alpha_+\cong(2q_c)^{1/2}$ so that Eqs. (2.26) give

$$M_{cv}(\mathcal{E}_c,\mathcal{E}_v)\cong\left(\frac{m_v}{\pi\hbar^2}\right)^{1/2}\frac{2i(k_vq_c)^{1/2}}{q_c^2+k_v^2}, \tag{2.27b}$$

which is the form of (2.26a) we use in the next section to illustrate the character of the contribution of vertical interband transitions to the absorption coefficient.

III. OPTICAL ABSORPTION

A. General Formulas

The expression for the optical-absorption coefficient (per unit volume), $\alpha(\omega)$, is given by[26]

$$\alpha(\omega)=\frac{4\pi^2e^2}{n'cm^2\omega}\sum_f|P_{fi}|^2\delta(E_f-E_i-\hbar\omega), \tag{3.1}$$

in which i denotes the initial state of the system with no excitation, f denotes the final state with an electron-hole pair, n' is the optical dielectric constant, ω is the angular frequency of the incident light and P_{fi} is the momentum matrix element[25,27]

$$P_{fi}=\sum_{\mathbf{k}_e\mathbf{k}_h}\Psi_{\mathbf{k}_e,\mathbf{k}_h,j,j'}I_{jj'}(\mathbf{k}_e,\mathbf{k}_h,\xi,\mathbf{q}), \tag{3.2a}$$

$$I_{jj'}(\mathbf{k}_e,\mathbf{k}_h,\xi,\mathbf{q})=\frac{\hbar}{i}\int d^3r\,\psi_{\mathbf{k}_ej}^\dagger(\mathbf{r})e^{i\mathbf{q}\cdot\mathbf{r}}\xi\cdot\nabla\psi_{\mathbf{k}_h,j'}(\mathbf{r}). \tag{3.2b}$$

The wave vector of the incident light is denoted by $\mathbf{q}$ and its polarization vector by ξ. As in previous sections, the $\psi_{\mathbf{k},j}(\mathbf{x})$ denote the Bloch functions associated with the jth band. We always use the dipole approximation and set $\mathbf{q}=0$ in Eqs. (3.2).

[25] C. B. Duke and M. E. Alferieff, Phys. Rev. **145**, 583 (1966).

[26] J. Bardeen, F. J. Blatt, and L. H. Hall, in *Photoconductivity Conference* (John Wiley & Sons, Inc., New York, 1956), p. 146.

[27] R. J. Elliott, Phys. Rev. **108**, 1384 (1957).

In the subsequent sections we consider both the interband transitions between localized conduction-band states and the valence band ($j=c$, $j'=v$) and intraband transitions among the localized states themselves ($j=j'=c$). Electron-hole (exciton) correlations[25,27] are neglected. These correlations have been studied in two-dimensional systems by other authors.[19] Using this approximation, the coefficients in (3.2a) become

$$\Psi_{\mathbf{k}_e,\mathbf{k}_h,j,j'}=f_{j,E_j}^{\dagger}(\mathbf{k}_e)f_{j',E_{j'}}(\mathbf{k}_h)\,, \tag{3.3a}$$

$$E_j-E_{j'}=E_f\,, \tag{3.3b}$$

$$f_{j,E}(\mathbf{k})=\frac{1}{N^{1/2}}\int d^3r\, e^{-i\mathbf{k}\cdot\mathbf{r}}f_{j,E}(\mathbf{r})\,. \tag{3.3c}$$

The envelope functions $f_{j,E}(\mathbf{r})$ are given by (2.3) and (2.21) for the conduction and valence bands, respectively, in the case of an accumulation region in the conduction band near the semiconductor interface.

In parts B and C of this section, we apply Eqs. (3.1)–(3.3) to calculate the absorption coefficient $\alpha(\omega)$ for interband and intraband transitions, respectively.

B. Interband Transitions

We consider only (vertical) dipole transitions which are "allowed" in Elliot's notation.[27] For interband transitions we apply the customary approximation[13,25,27] that matrix element (3.2b) is given by

$$I_{cv}=\delta_{\mathbf{k}_e,\mathbf{k}_h}C_0(\xi)\,, \tag{3.4a}$$

$$C_0=\int_B d^3r\,\psi_{0c}^{\dagger}(\mathbf{r})\xi\cdot\mathbf{p}\psi_{0v}(\mathbf{r})\,, \tag{3.4b}$$

as long as one considers absorption near the interband threshold. The integral in (3.4b) is over a unit cell of volume B. Equations (3.4) are applicable to the direct edge in group IV and III–V semiconductors, and in particular to GaAs, for which the localized-state binding energies were evaluated in the previous section. Insertion of (3.4) into (3.2a) gives

$$P_{fi}=C_0\int d^3r\, f_{c,E_c}(\mathbf{r})f_{v,E_v}(\mathbf{r})$$

$$=C_0\delta_{k_{\|c},k_{\|v}}M_{cv}(\mathcal{E}_c,\mathcal{E}_v)\,, \tag{3.5}$$

in which M_{cv} is given by Eqs. (2.26) and (2.27). The absorption coefficient α_L for absorption into unoccupied two-dimensional localized-state bands is given by

$$\alpha_L(\omega)=\frac{2\pi e^2|C_0|^2(\mu_{11,1}\mu_{11,2})^{1/2}}{n'cm^2\omega\hbar^2}\times\sum_i G(\omega,\mathcal{E}_{ci})\Theta(\hbar\omega-E_g+\mathcal{E}_{ci})\,, \tag{3.6a}$$

$$G(\omega,\mathcal{E}_{ci})=\int_0^{\hbar\omega-E_g+\mathcal{E}_{ci}}|M_{cv}(\mathcal{E}_{ci},\mathcal{E})|^2d\mathcal{E}\,, \tag{3.6b}$$

$$\frac{1}{\mu_i}=\frac{1}{m_{c,i}}+\frac{1}{m_{v,i}}\,. \tag{3.6c}$$

The total absorption coefficient is obtained by adding to (3.6a) those contributions due to transitions to continuum states in the conduction band which, however, enter only for $\hbar\omega>E_g$ when exciton correlations are neglected.

From Eqs. (3.6) we see that the analog of the Franz-Keldysh effect in an inhomogeneous electric field near an interface introduces a series of broadened steps in $\alpha_L(\omega)$ below the interband threshold. These steps are caused by transitions from the valence band to the two-dimensional bands associated with localized states in an accumulation region near the interface. They are described by the spectral function, $G(\omega,\mathcal{E}_{ci})$, and are sharp only in the limit that $m_v\gg m_c$; i.e., that the valence band is much more flat than the conduction band for n-type accumulation regions and vice versa for p-type accumulation regions. This result may be illustrated by considering the approximation (2.27) to M_{cv} in which case, for spherical bands, we find

$$G(\omega,\mathcal{E}_{ci})\cong\frac{2}{\pi}(r_m\mathcal{E}_{ci})^{1/2}\int_0^{\hbar\omega-E_g+\mathcal{E}_{ci}}\frac{\mathcal{E}^{1/2}d\mathcal{E}}{(\mathcal{E}+r_m\mathcal{E}_{ci})^2}\,,$$

$$=\frac{2}{\pi}\Bigg[\tan^{-1}\left(\frac{\hbar\omega-E_g+\mathcal{E}_{ci}}{r_m\mathcal{E}_{ci}}\right)^{1/2}-\frac{[(r_m\mathcal{E}_{ci})(\hbar\omega-E_g+\mathcal{E}_{ci})]^{1/2}}{\hbar\omega-E_g+\mathcal{E}_{ci}+r_m\mathcal{E}_{ci}}\Bigg]\,, \tag{3.7a}$$

$$r_m\equiv m_c/m_v\,. \tag{3.7b}$$

Denoting by $x\equiv(\hbar\omega-E_g+\mathcal{E}_{ci})/\mathcal{E}_{ci}$ the normalized energy above the threshold, we see that $G(x,\mathcal{E}_{ci})$ approaches its maximum value of 1 below the band edge ($x<1$) only when $r_m\ll1$. This result is shown graphically in Fig. 9. As for light holes in GaAs $r_m\sim0.7$.[28] The structure introduced by the localized states will be hard to distinguish from the inhomogeneous strain broadening of the direct edge. Absorption from the heavy-hole band exhibits $r_m\sim0.175$ with correspondingly sharper structure.

For those localized states which are occupied, the contribution to the sum in (3.1) vanishes because it is weighted by a $[1-n(E_c)]n(E_v)$ factor. This result has the consequence that (3.6a) becomes

$$\alpha_L(\omega)=\frac{2\pi e^2|C_0|^2}{n'm^2\omega\hbar^2}(\mu_{11,1}\mu_{11,2})^{1/2}\sum G(\omega,\mathcal{E}_{ci})\times[\Theta(-E_F-\mathcal{E}_{ci})\Theta(\hbar\omega-E_g+\mathcal{E}_{ci})+\Theta(E_F+\mathcal{E}_{ci})\Theta(\hbar\omega-E_g-E_F)]\,. \tag{3.6d}$$

[28] J. W. Conley and G. D. Mahan, General Electric Research and Development Center Report No. 66-C-443 (to be published).

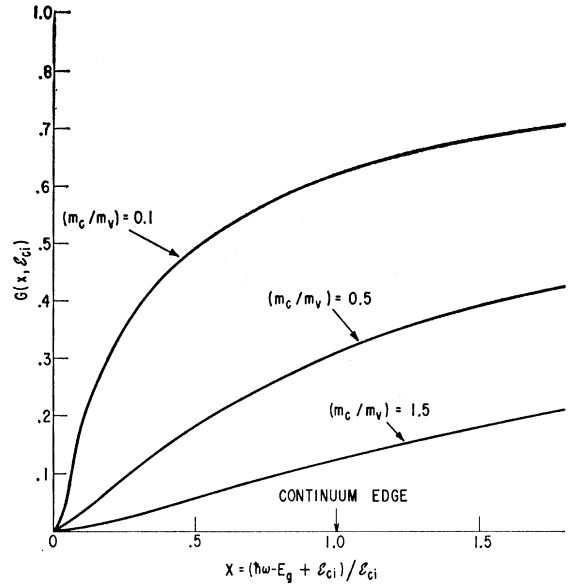

FIG. 9. The spectral weight $G(x,\mathcal{E}_{ci})$ for interband transitions calculated from Eqs. (3.7) in the text for various mass ratios $r_m=(m_c/m_v)$ associated with spherical energy bands.

The second term indicates that although $G(\omega,\mathcal{E}_{ci})$ may rise gradually, if the localized-state band is occupied, no absorption occurs until $\hbar\omega\geq\hbar\omega_0\equiv E_g+E_F$ so that a sharp onset of the absorption, analogous to the Burstein edge in a bulk-degenerate semiconductor, occurs at $\omega=\omega_0$ with strength $G(\omega_0,\mathcal{E}_{ci})$.

An attractive interaction between the electron and hole sharpens all the absorption edges[29,30] in addition to introducing bound-state (exciton) peaks. Therefore the structure predicted in this section will be made more pronounced by electron-hole correlations.

Finally, the contributions to the absorption illustrated in Fig. 9 exhibit the same qualitative features as those due to transitions from the valence band to sharp "conventional" localized surface states.[14,16] This result is a consequence of the similarity between the wave function of such a state and that of a tightly bound, space-charge-induced state. For transitions from the valence band to the "conventional" surface states, the imposition of an ac modulation of the field-plate bias affects the absorption coefficient only by modulating the valence-band space-charge potential. Thus when the change in α induced by the shift in the valence-band edge is detected in phase with the modulating voltage, the effective $\Delta\alpha$ measured is that due to a shift of an absorption edge like those shown in Fig. 9. As expected, such a $\Delta\alpha$ has the form attributed by Harrick[16] to his type-2 transitions. The $\Delta\alpha$ obtained for transitions between the localized states and the valence band is also due to a shift of the absorption bands shown in Fig. 9. However, this shift is not as large as that for a surface state of fixed energy because the localized-state energy is altered by changes in the space-charge potential. The oscillator strength of the transition also is modified in accordance with Eqs. (3.6) and (3.7).

C. Intraband Transitions

In calculating the momentum matrix elements (3.2) for intraband transitions, one uses the theorem[31] that

$$\int d^3x\,\psi_{\mathbf{k}j}^{\dagger}(\mathbf{x})p_\beta\psi_{\mathbf{k}j}(\mathbf{x})=\frac{m}{\hbar}\frac{\partial\epsilon_j(\mathbf{k})}{\partial k_\beta} \tag{3.8}$$

to relate the dipole matrix element (3.2a) directly to the envelope function. For vertical transitions among the two-dimensional localized-state bands associated with the βth mass ellipsoid one finds[20]

$$P_{fi}=\sum_{s,t}\xi_s\left(\frac{m}{m^*}\right)_{st}^{(\beta)}\int d^3x\,\bar{f}_{Ef}(\mathbf{x})p_t f_{Ei}(\mathbf{x}), \tag{3.9}$$

in which $(1/m^*)_{st}$ is the effective-mass tensor for the ellipsoid. Using Eqs. (2.3) we see that in the dipole approximation (vertical transitions), for which (3.9) is relevant, one finds the selection rule that only the component of the polarization vector ξ normal to the plane of the junction causes transitions. For this polarization, the momentum matrix element becomes

$$P_{fi}^{x}=\frac{i\hbar m}{m_{\perp,c}^{(\beta)}}\alpha_+(p_{cf})\alpha_+(p_{ci})I_3(-p_{cf},-p_{ci}), \tag{3.10}$$

in which I_3 is given by Eq. (A14) in the Appendix. Using the approximation (2.14), which is comparable to the use of Eqs. (3.7) for interband transitions, we find that we should use

$$|P_{fi}^{(\beta)}|^2=|P_{fi}^{x(\beta)}|^2\delta_{\mathbf{k}_{\parallel f},\mathbf{k}_{\parallel i}}, \tag{3.11a}$$

$$|P_{fi}^{x(\beta)}|^2=16\hbar^2\left(\frac{m}{m_{c,\perp}^{(\beta)}}\right)^2\left[\frac{q_{ci}^{(\beta)}q_{cf}^{(\beta)}}{q_{ci}^{(\beta)}+q_{cf}^{(\beta)}}\right]^2 \tag{3.11b}$$

in Eq. (3.1). In the case that more than one localized-state band is occupied, the strength of the transition between the localized levels is reduced, but, unlike the case of interband transitions, there is no Burstein shift of the edge.

Taking into consideration the fact that in a many-valley semiconductor the intraband transitions associated with each valley are independent in the effective-mass approximation, we find that the absorption co-

[29] Y. Toyazawa, M. Inoue, T. Inui, M. Okazaki, and E. Hanamura, J. Phys. Soc. Japan **21**, 209 (1966).
[30] J. J. Hopfield, Tokyo Summer Institute for Theoretical Physics, 1966 (to be published).
[31] See, e.g., E. Spenke, *Electronic Semiconductors* (McGraw-Hill Book Company, Inc., New York, 1958), p. 205.

efficient is generally given by

$$\alpha(\omega)=\frac{4\pi^2e^2}{n'cm^2\omega\hbar^2}\sum_{\beta}\rho_{11}{}^{(\beta)}\sum_{f,i}|P_{fi}{}^{x(\beta)}|^2 \times\Theta(\hbar\omega-\mathcal{E}_{cf}{}^{(\beta)}+\mathcal{E}_{ci}{}^{(\beta)})\Theta(\mathcal{E}_{ci}{}^{(\beta)}+E_F) \times[(\mathcal{E}_{ci}{}^{(\beta)}+E_F)\Theta(-\mathcal{E}_{cf}{}^{(\beta)}-E_F) +(\mathcal{E}_{ci}{}^{(\beta)}-\mathcal{E}_{cf}{}^{(\beta)})\Theta(\mathcal{E}_{cf}{}^{(\beta)})], \quad (3.12)$$

in which $\rho_{11}{}^{(\beta)}$ is given by Eq. (2.16d). From Eqs. (3.11) and (3.12) we see that small $m_{\perp,c}$ and large binding of the individual localized states (i.e., large q_{ci}, q_{cf}) favor strong transitions. The spectral form of $\alpha(\omega)$ is a series of step functions, as expected for a genuine two-dimensional system.

D. Summary

Equations (3.6) and (3.12) give the contribution to the absorption coefficient due to transitions from the valence band to localized states in the conduction band and due to transitions among localized conduction-band states, respectively. The absorption edges in $\alpha(\omega)$ due to transitions to localized states from the valence band are broadened considerably due to the continuum character of the valence-band eigenstates and the small oscillator strengths associated with the continuum eigenstates near the band edge. Only if the binding energy of the localized state is much larger than that of an exciton and $(m_c/m_v)\ll 1$ is this structure in $\alpha(\omega)$ likely to be distinguishable from the inhomogeneous strain broadening and bulk exciton affects at the direct absorption edge. The structure in $\alpha(\omega)$ in the infrared region ($\Delta E\sim$10–25 meV) consists of a series of steps characteristic of the density of states in two-dimensional systems. The positions and dipole strengths of these steps scale with field-plate bias. Equations (3.12) and the considerations of Secs. IIA and IIB permit a quantitative analysis of the strength and scaling of these contributions to $\alpha(\omega)$ for any given bulk and surface parameters of a given sample. Experimental observation of this scaling of the predicted structure in either $\alpha(\omega)$ or $\Delta\alpha(\omega)$ with field-plate bias would provide an unambiguous verification of the existence of quantized states in narrow accumulation or inversion regions.

Finally, our analysis also can be applied to describe the influence of quantization effects on the energy dependence near threshold of photoemission across the oxide barrier in the case that the photoemitted electrons originate in the space-charge regions. For a p-type accumulation region, the direct, surface-emission threshold energy is raised by distance of the most tightly bound hole from the top of the valence band.

Note added in proof. The above analysis also forms the basis of a model for calculating line shapes in surface-barrier electroreflectance[32] in cases for which the space-charge potential can be determined and subsequently approximated by an exponential. An important consequence of the model is the possibility of optical frequency transitions between occupied quantized-state bands and either quantized or continuum states associated with higher-energy bands. These transitions lead to edges in $\alpha(\omega)$ which exhibit a strong dependence on the surface potential, crystal face, and temperature. Therefore interpretations of measured peaks[32] must be regarded as tentative until the experimental results are correlated with a detailed model of the space-charge potential on the basis of which surface effects can be eliminated as the mechanism for these peaks. Such a detailed analysis is of particular importance near the 3.5-eV spectral region in Silicon where the interpretations of the electroreflectance[36] and piezoreflectance[33] data differ substantially.

[32] B. O. Seraphin, Phys. Rev. **140**, A1716 (1965).

ACKNOWLEDGMENTS

The author is indebted to Dr. W. Engeler, Dr. M. Garfinkel, and Dr. F. Ham for stimulating discussions.

APPENDIX: EXPANSIONS OF INTEGRALS INVOLVING THE $F(Q^2,g,p,x)$

Let us first consider the normalization

$$I_1(-p,-p)=\int_0^\infty|F(-Q^2,g,-p,x)|^2dx. \quad (A1)$$

The general procedure we use to evaluate all such integrals is to use the relations between the F and Bessel functions:

$$F(-Q^2,g,-p,x)=\frac{\Gamma(p+1)}{(Q/g)^p}J_p(2Qe^{-gx/2}/g), \quad (A2a)$$

$$F(Q^2,g,-p,x)=\frac{\Gamma(p+1)}{(Qe^{-i\pi/2}/g)^p} \times J_p\left(2Q\exp\left[\frac{i\pi-gx}{2}\right]\Big/g\right) \quad (A2b)$$

and the expansion of products of Bessel functions[34]

$$J_p(ax)J_{p'}(bx)=\frac{(ax/2)^p(bx/2)^{p'}}{\Gamma(p'+1)} \times\sum_{m=0}^{\infty}\frac{(-a^2x^2/4)^m\,{}_2F_1(-m,-p-m,p'+1,b^2/a^2)}{m!\Gamma(p+m+1)}, \quad (A3a)$$

$${}_2F_1(a,b,c,x)=\sum_{n=0}^{\infty}\frac{(a)_n(b)_nx^n}{n!(c)_n}, \quad (A3b)$$

$$(a)_n\equiv 1\times a\times(a+1)\times\cdots\times(a+n). \quad (A3c)$$

[33] G. W. Gobeli and E. O. Kane, Phys. Rev. Letters **15**, 142 (1965).

[34] G. N. Watson, *Theory of Bessel Functions* (Cambridge University Press, London, 1945), p. 148.

The hypergeometric function ${}_2F_1$ occurring in (A3a) is a polynomial in (b^2/a^2) of order m. In the case that $p=p'$, $a=b$, Eq. (A3) reduces to[35]

$$J_p{}^2(x)=\left(\frac{x}{2}\right)^{2p} \times\sum_{m=0}^{\infty}\frac{(-x^2/4)^m\Gamma(2p+2m+1)}{m!\Gamma(2p+m+1)[\Gamma(p+m+1)]^2}. \quad \text{(A4)}$$

Use of (A2a) and (A4) gives the product expansion for the F functions:

$$F^2(-Q^2, g, -p, x)=\exp(-pgx)\cdot\sum_{m=0}^{\infty}\frac{1}{m!} \times\left(\frac{-Q^2e^{-gx}}{g^2}\right)^m\frac{\Gamma(2p+2m+1)}{\Gamma(2p+m+1)}\left[\frac{\Gamma(p+1)}{\Gamma(p+m+1)}\right]^2. \quad \text{(A5)}$$

Equation (A5) can be readily integrated to give

$$I_1(-p, -p)=\frac{2}{g}\sum_{m=0}^{\infty}\frac{1}{m!}\left(\frac{-Q^2}{g^2}\right)^m\frac{\Gamma(2p+2m)}{\Gamma(2p+m+1)} \times\left[\frac{\Gamma(p+1)}{\Gamma(p+m+1)}\right]^2. \quad \text{(A6)}$$

A closely related integral to I_1 is the overlap integral between conduction band and valence band F functions:

$$I_2(-Q_c{}^2, -p_c; Q_v{}^2, ip_v) =\int_0^{\infty}dxF(-Q_c{}^2, g, -p_c, x)F(Q_v{}^2,g,ip_v,x). \quad \text{(A7)}$$

Use of (A2) in (A3) gives the product expansion

$$F(-Q_c{}^2, g, -p_c, x)F(Q_v{}^2,g,ip_v,x) =\exp\left[(-p_c+ip_v)\cdot\frac{gx}{2}\right]\sum_{m=0}^{\infty}\frac{1}{m!}\left(\frac{Q_v{}^2e^{-gx}}{g^2}\right)^m \times\frac{\Gamma(-ip_v+1)}{\Gamma(-ip_v+m+1)}{}_2F_1(-m, ip_v-m; p_c+1, -Q_c{}^2/Q_v{}^2), \quad \text{(A8a)}$$

which when integrated gives

$$I_2(-Q_c{}^2, -p_c; Q_v{}^2, ip_v)=\frac{2}{g}\sum_{m=0}\frac{(Q_v{}^2/g^2)^m}{(p_c-ip_v+2m)} \times\frac{\Gamma(-ip_v+1)}{\Gamma(-ip_v+m+1)}{}_2F_1(-m, ip_v-m, p_c+1, -Q_c{}^2/Q_v{}^2). \quad \text{(A8b)}$$

[35] Reference 32, p. 147.

The fact that in general $m_{\perp,c}\ll m_{\perp,v}$ has the consequence that $(Q_c/Q_v)^2\ll 1$ in the hypergeometric function in (A8b).

Our final integral is that needed in the calculation of the oscillator strength of transitions between localized states:

$$I_3(-p_1, -p_2)=\int_0^{\infty}F(-Q^2, g, -p_1, x) \times(dF/dx)(-Q^2, g, -p_2, x)dx. \quad \text{(A9)}$$

For the evaluation of this integral it is most convenient to make the neglect of the $x<0$ terms in the integral rigorous by taking the $V_b\to\infty$ limit in the text. In this limit we see from (A2) and (2.9d) in the text:

$$J_{p_1}(2Q/g)=J_{p_2}(2Q/g)=0. \quad \text{(A10)}$$

Using (A2) and the identity[36]

$$J_p{}'(u)=J_{p-1}(u)-(p/u)J_p(u), \quad \text{(A11)}$$

we obtain, by making the variable substitution $u=(2Qe^{-gx/2}/g)$ in (A9), the result

$$I_3(-p_1, -p_2)=\frac{\Gamma(p_1+1)\Gamma(p_2+1)}{(Q/g)^{p_1+p_2}} \times\int_0^{2Q/g}J_{p_1}(u)\left[J_{p_2}(u)-\frac{p_2}{u}J_{p_2}(u)\right]du. \quad \text{(A12)}$$

The integral of the last term in the integrand in (A12) can be performed explicitly[37] and vanishes due to the quantization condition (A10) if p_1, p_2 are not both zero. Using another limiting case[33] of (A3), i.e.,

$$J_{p_1}(x)J_{p_2}(x) =\sum_{m=0}^{\infty}\frac{(-)^m(x/2)^{p_1+p_2+2m}\Gamma(p_1+p_2+2m+1)}{m!\Gamma(p_1+p_2+m+1)\Gamma(p_1+m+1)\Gamma(p_2+m+1)}. \quad \text{(A13)}$$

We obtain, after integrating in (A12), the final result:

$$I_3(-p_1, -p_2)=2p_2\sum_{m=0}^{\infty}\frac{1}{m!}\left(\frac{-Q^2}{g^2}\right)^m \times\frac{\Gamma(p_1+p_2+2m)}{(p_1+p_2+2m)\Gamma(p_1+p_2+m)}\frac{\Gamma(p_1+1)}{\Gamma(p_1+1+m)} \times\frac{\Gamma(p_2)}{\Gamma(p_2+m)}. \quad \text{(A14)}$$

[36] Reference 32, p. 83.
[37] Reference 32, p. 135.